

See discussions, stats, and author profiles for this publication at: <https://www.researchgate.net/publication/231390701>

Copper Promoted Cobalt and Nickel Catalysts Supported on Ceria–Alumina Mixed Oxide: Structural Characterization and CO Oxidation Activity

ARTICLE *in* INDUSTRIAL & ENGINEERING CHEMISTRY RESEARCH · SEPTEMBER 2009

Impact Factor: 2.59 · DOI: 10.1021/ie900755b

CITATIONS

40

READS

35

3 AUTHORS:



[Benjaram M Reddy](#)

CSIR-Indian Institute of Chemical Technolo...

280 PUBLICATIONS 5,558 CITATIONS

[SEE PROFILE](#)



[Komateedi N Rao](#)

Heesung Catalyst

30 PUBLICATIONS 553 CITATIONS

[SEE PROFILE](#)



[Pankaj Bharali](#)

Tezpur University

38 PUBLICATIONS 618 CITATIONS

[SEE PROFILE](#)

Copper Promoted Cobalt and Nickel Catalysts Supported on Ceria–Alumina Mixed Oxide: Structural Characterization and CO Oxidation Activity

Benjaram M. Reddy,* Komateedi N. Rao, and Pankaj Bharali

Inorganic and Physical Chemistry Division, Indian Institute of Chemical Technology,
Uppal Road, Hyderabad–500 607, India

Catalytic activity of CoO, NiO, CuO–CoO, and CuO–NiO nanocrystalline mono- and bimetallic catalysts over a thermally stable and high surface area ceria–alumina mixed oxide support was evaluated for oxidation of carbon monoxide at normal atmospheric pressure and lower temperatures. The content of Co or Ni in the respective monometallic catalysts was 10 wt % and the Cu-promoted samples contained 5 wt % each. These catalysts were prepared by a wet impregnation procedure and the CeO₂–Al₂O₃ support was obtained by a deposition precipitation method. The synthesized catalysts were characterized by BET surface area, X-ray diffraction (XRD), energy dispersive X-ray microanalysis (EDX), temperature-programmed reduction (TPR), transmission electron microscopy (TEM), and X-ray photoelectron spectroscopy (XPS) techniques. XRD patterns of 773 K calcined samples revealed the presence of metal oxide phases, namely, CeO₂, CuO, NiO, and Co₃O₄ in the respective catalysts. However, after calcination at 1073 K, the XRD lines corresponding to CuO and NiO were absent. EDX results confirmed the actual amount of metal loadings in the respective catalysts. The H₂-TPR results suggested that Cu-doping accelerates and decreases the onset reduction temperature of monometallic samples. Raman results of 773 K calcined samples showed a prominent broad peak at 461 cm^{−1} corresponding to the F_{2g} Raman active mode of CeO₂. The TEM studies confirmed the presence of nanosized composite oxides with narrow size distribution of metal oxide particles. The XPS results disclosed the presence of Cu¹⁺ species along with Cu²⁺ and the promotional effect of Cu in Co-containing samples to suppress the formation of the CoAl₂O₄ phase. Among different catalysts, the copper promoted CuO–NiO/CeO₂–Al₂O₃ sample exhibited better activity for CO oxidation at lower temperatures. The better activity of the catalyst is attributed to the formation of well-dispersed and highly reducible metal oxide species over the mixed oxide support.

1. Introduction

Design of efficient catalysts for oxidation of carbon monoxide at low temperatures is an important and most demanding research topic during the last several years.^{1–3} The catalytic oxidation of CO is most significant subject due to its eventual applications in different areas of chemical research. Particularly, these applications include air-purification devices for respiratory protection, pollution control devices for reducing industrial and environmental emissions, removal of trace quantities of CO from the ambient air in enclosed atmospheres such as submarines and space craft, and carbon dioxide lasers.³ The CO gas sensors also work based on the catalytic materials employed for CO oxidation. Among the different metal oxides used either as active components or as the supports for CO oxidation, ceria (CeO₂) is one of the most attractive and widely employed materials. The CeO₂ is the oxide of the rare-earth metal cerium, which may exist in various compositions, due to the capacity of ceria to switch between two oxidation states Ce³⁺ and Ce⁴⁺. For CO oxidation, ceria has been reported to lower the activation energy, increase the reaction rate, and suppress the usual CO inhibition effect.^{2,4} However, it is known that noble metals are highly active for oxidation of CO at lower temperatures. In addition, supported platinum catalysts were extensively investigated by several authors for this purpose. For instance, Pt/Al₂O₃,⁴ Pt/CoO_x/SiO₂,⁵ Pt/A-zeolite,⁶ Pt/mordenite,⁷ and various other combinations were examined for CO oxidation. Recently, it has been disclosed that highly dispersed gold nanoparticles sup-

ported on metal oxides are very active for CO oxidation at low temperatures, even below room temperature.^{8,9} However, it was observed that supported gold catalysts deactivate much rapidly than the corresponding platinum catalysts.⁹ The efficiency of noble metals at higher temperatures is still in debate since they promote methane formation and poisoned by CO₂ owing to the formation of carbonate species on the catalyst surface. Therefore, the development of an efficient non-noble metal based catalyst for oxidation of CO is still a promising area of catalysis research.

Transition metal oxides or mixed oxides have been established as inexpensive alternatives to precious metal and noble metal containing catalysts. Many recent studies revealed that activity of ceria and ceria-containing catalysts in oxidation reactions is greatly enhanced not only by precious metals, but also by base metals.^{10–12} Among them, copper/ceria combination appears to be a potential catalyst for various oxidation reactions, such as total oxidation of CO, methanol, and methane.^{4,13–15} Liu and Flytzani-Stefanopoulos¹⁶ have reported that CuO–CeO₂ catalysts are very active for oxidation of CO exhibiting a high specific activity several orders of magnitude higher than that of the conventional Cu-based catalysts and at significantly lower operating temperatures. The role of ceria as a support for base metals is not only related to its oxygen storage/release capacity (OSC) but also to the ability of improving dispersion of metals.^{4,16–18} Ceria provides the unique capability of promoting oxidation reactions, due to its easy generation of oxygen vacancies to form interfacial active centers. The surface oxygen vacancies of doped ceria and facile Ce⁴⁺/Ce³⁺ redox reaction are believed to be the driving force for this unique behavior.

* To whom correspondence should be addressed. Tel.: +91 40 27191714. Fax: +91 40 27160921. E-mail addresses: bmreddy@iict.res.in; mreddyb@yahoo.com.

As a consequence, the metal–support interaction has also been established to explain the high catalytic performance in various reactions.

The basic idea in undertaking this work was to exploit the advantages of ceria, and particularly, its ability to store oxygen, while improving its resistance to sintering. Thus, the use of ceria–alumina (CA) mixed oxide as a catalyst support is expected to exhibit better thermal stability and extend the operating temperature range of the catalyst, and hence, it can be considered as the best choice to achieve high CO conversions.^{19–24} Recently, Kang et al.²⁵ and Mariño et al.²⁶ examined the CO oxidation over various CeO₂ supported metal oxides such as cobalt, copper, manganese, nickel, chromium, iron, and vanadium. They conclude that Cu-based catalysts exhibit best results for CO oxidation, whereas Co and Ni containing catalysts show moderate activity. It is also known from the literature that a single component base metal catalyst cannot rival a precious metal catalyst. Therefore, to improve their catalytic activity, attempts have been made by combining various elements together. The present investigation was undertaken based on the aforesaid ideas to explore the significance of interactions between the active metal and the supporting metal oxides. For this purpose, copper promoted Ni and Co bimetallic catalysts supported over ceria–alumina were prepared and characterized using thermal analysis (TGA/DTA), BET surface area, X-ray diffraction (XRD), Raman spectroscopy, temperature-programmed reduction (TPR), energy dispersive X-ray microanalysis (EDX), transmission electron microscopy (TEM), and X-ray photoelectron spectroscopy (XPS) techniques. The prepared catalysts were evaluated for oxidation of carbon monoxide at normal atmospheric pressure and temperatures below 773 K.

2. Experimental Section

2.1. Catalyst Preparation. The CeO₂–Al₂O₃ (CA) mixed oxide (1:1 mol ratio based on oxides) was prepared by a deposition precipitation method. In a typical preparation, finely powdered alumina (Harshaw Chem.) was employed as the source of Al₂O₃ and ammonium cerium(IV) nitrate (Fluka) as the precursor for CeO₂. A more detailed description of the support preparation procedure can be found elsewhere.²¹ The CA mixed oxide calcined at 773 K was used as the support for the synthesis of monometallic and bimetallic samples. The monometallic samples with 10 wt % CoO and NiO over CA were synthesized by a wet impregnation method, and bimetallic catalysts with 5 wt % each CuO–CoO and CuO–NiO over CA were prepared by simultaneous-impregnation method. To impregnate the corresponding metals over the support, an adequate amounts of aqueous nickel nitrate (Ni(NO₃)₂·6H₂O), cobalt nitrate (Co(NO₃)₂·6H₂O), and copper nitrate (Cu(NO₃)₂·3H₂O) solutions were used. To the aqueous solutions of metal precursors, the finely powdered CA support calcined at 773 K was added. The excess water was gradually evaporated on a hot water-bath under constant mechanical agitation, subsequently dried at 373 K for 10 h. Finally, the obtained materials were calcined at 773 and 1073 K for 5 h in a closed muffle furnace.

2.2. Catalyst Characterization. X-ray Diffraction. The X-ray powder diffraction patterns were acquired with a Rigaku Multiflex instrument equipped with Ni-filtered Cu K α radiation source and a scintillation counter detector (SCD). Crystalline phases were identified by matching the experimental patterns with the Powder Diffraction File-International Centre for Diffraction Data (PDF-ICDD). The mean crystallite size (D_{XRD})

was measured by employing Scherrer equation using the most prominent ceria peak (111).

Raman Spectra. The Raman spectra were recorded with a Horiba Jobin Yvon HR 800 Raman spectrometer at ambient temperature. The emission line at 514 nm from Ar⁺ laser (Spectra Physics) was focused on the sample under the microscope. The time of acquisition was adjusted according to the intensity of Raman scattering. The power of the incident beam on the sample was 3 mW. The wavenumber values reported from the spectra are accurate to within 2 cm⁻¹. In order to ascertain the homogeneity of the sample, spectra were recorded at various points and compared. All samples were found to be highly homogeneous.

Temperature Programmed Reduction. H₂-TPR measurements were carried out on a Micromeritics Auto Chem 2910 instrument with a thermal conductivity detector (TCD). The sample was treated with flowing He at 473 K for 90 min before the run. The measurements were performed using 5% H₂/Ar gas flow of 30 mL/min and about 150 mg of sample, with the heating rate of 10 K/min.

Transmission Electron Microscopy. TEM investigation was performed using a Tecnai-12, FEI electron microscope with 2 Å point-to-point resolution. The samples were supported on a carbon grid by dropping ethanol suspensions containing the uniformly dispersed powers.

Thermal Analysis. The differential thermal analysis–thermogravimetric analysis (DTA-TGA) measurements were made on a Mettler Toledo TG-SDTA apparatus. The sample was heated from ambient to 1273 K under nitrogen flow and the heating rate was 10 K/min. In a typical measurement, the weight of the sample was ca. 8–12 mg.

BET Surface Area. The specific surface area measurements were made using a Gemini 2360 Instrument by N₂ physisorption at liquid nitrogen temperature. Prior to analysis, samples were degassed at 393 K under vacuum for 12 h to remove any residual moisture and other volatiles.

Energy Dispersive X-ray Microanalysis (EDX). To know the surface composition of metal ions present in the samples, the EDX microanalysis was performed. The elemental analyses were carried out on a Kevex, Sigma KS3 EDX instrument operating at a detector resolution of 137 eV.

X-ray Photoelectron Spectroscopy. The XPS measurements were made on a KRATOS (ESCA AXIS 165) spectrometer by using Mg K α (1253.6 eV) radiation as the excitation source. Charging of catalyst samples was corrected by setting the binding energy of the adventitious carbon (C 1s) at 284.6 eV. The finely ground oven-dried samples were dusted on a double stick graphite sheet and mounted on the standard sample holder. The sample holder was then transferred to the analysis chamber, which can house 10 samples at a time, through a rod attached to it. The samples were outgassed in a vacuum oven overnight before XPS measurements. Quantitative analysis of the atomic ratios was accomplished by determining the elemental peak areas, following a Shirley background subtraction by the usual procedures documented in the literature.^{27,28}

2.3. Activity Studies. The CO oxidation activity of different samples was evaluated at normal atmospheric pressure and temperatures in the range of 300–773 K in a fixed bed microreactor at a heating ramp of 5 K/min. About 100 mg catalyst sample (250–355 μm sieve fraction) diluted with quartz particles of the same size was placed in a quartz reactor for evaluation. Temperature was measured directly at the catalyst bed, using a thermocouple placed near the catalyst bed. The CO and CO₂ gas concentrations during the reaction were

measured using an Uras 14 infrared analyzer module, and the O₂ concentration was measured using a Magnos 16 analyzer (Hartmann & Braun). Prior to oxidation of CO, catalysts were heated to 773 K in 10.2% O₂/Ar gas mixture, using a heating ramp of 10 K/min, and kept at the final temperature for 1 h. The oxidized sample was then purged in argon and cooled to the desired starting temperature. The CO/O₂ reactant feed ratio was 1, and partial pressures of CO and O₂ were in the range of 10 mbar. The conversion of CO to CO₂ was calculated using the following equation.^{10,23}

$$\text{CO conversion (\%)} = \frac{[\text{CO}]_{\text{in}} - [\text{CO}]_{\text{out}}}{[\text{CO}]_{\text{in}}} \times 100\%$$

3. Results and Discussion

3.1. Structural Characterization. To understand thermal stability and evolution of samples, the metal oxide impregnated catalysts were subjected to thermogravimetric analysis before calcination and the corresponding thermograms are presented in the Supporting Information (SI). As shown in the SI, the thermograms of all samples revealed three major weight loss peaks below 773 K. They exhibited a weight loss peak in the range 323–473 K with distinct peak intensities corresponding to the loss of nondissociative adsorbed water as well as water held on the surface of the samples by hydrogen bonding. The second thermal decomposition peak was primarily due to the loss of water held in the micropores of the mixed hydroxide/oxide gels and decomposition of nitrate species if remained during the preparation stage. At higher temperatures about 550 K, a weight loss peak was also observed which could be due to loss of water molecules by dehydroxylation of the surface hydroxyl groups. Further, the TG profile of CuO–CoO/CA sample showed a small weight loss signal at ~1100 K, which could be attributed to the loss of oxygen from Co₃O₄ to form CoO.^{29,30} Besides, the monometallic CoO/CA sample also showed the same peak nearly at 1130 K with very broad and low signal intensity, indicating that the addition of copper promotes the reducibility of Co₃O₄. Shaheen and Ali³¹ also noticed two thermal decomposition peaks at ~1073 and ~1223 K, due to reduction of Co₃O₄ to CoO and CuO to Cu₂O, respectively. Interestingly, no weight loss peak was observed in the present investigation corresponding to the transformation of CuO to Cu₂O, which indicates that the doped copper oxide may be in a +1 oxidation state or it is strongly interacting with the ceria support. However, CuO–NiO/CA did not show any high temperature weight loss peak. Hence, the thermograms of bimetallic CuO–CoO/CA and CuO–NiO/CA samples reveal that addition of Cu to NiO/CA and CoO/CA enhances the thermal stability of copper and also improves the reducibility of the second metal.

The activity of the catalytic system usually relates to its textural properties, particularly, the specific surface area and the crystallite size. On account of these considerations, the BET surface areas of various samples calcined at 773 and 1073 K are reported in Table 1. As can be noted from Table 1, all the samples exhibited high specific surface areas ranging from 140 to 165 m² g⁻¹, which is one of the most important requirements of metal oxide systems for catalytic applications. The CA support exhibited slightly higher surface area than the doped samples. The decrease in the surface area is mainly due to penetration of the dispersed metal oxides into the pores of the support and also owing to the formation of specific solid solutions as a result of interaction with the ceria.^{19–23} It has been found that calcination at higher temperatures is always

Table 1. BET Surface Area of Various Samples Calcined at 773 and 1073 K and Crystallite Size and Temperature at 50% CO Conversion ($T_{1/2}$) of Various Samples Calcined at 773 K

sample	BET SA (m ² g ⁻¹)		crystallite size (nm)	$T_{1/2}$ (K)
	773 K	1073 K		
CeO ₂ –Al ₂ O ₃ (CA)	164	64	3.7	
CoO/CA	145	64	5.9	527
NiO/CA	142	61	6.2	462
CuO–NiO/CA	145	54	7.1	364
CuO–CoO/CA	140	52	7.2	392

accompanied by an increase in the mean particle diameter and decrease in the specific surface area due to blocking of the pores. The crystallite size (D_{XRD}) of CeO₂ in various samples calcined at 773 K is summarized in Table 1. As can be noted from Table 1, the crystallite size of CeO₂ in all samples ranges from 3.5 to 7 nm. The extent of crystallite growth is greater in the case of metal oxide impregnated samples. This indicates that impregnated metal oxides accelerate the grain growth of ceria in CA support.³²

The X-ray powder diffraction patterns of various samples calcined at 773 and 1073 K are presented in Figure 1. As can be observed, all samples exhibited broad diffraction lines due to distinct fluorite-type structure of ceria. However, the absence

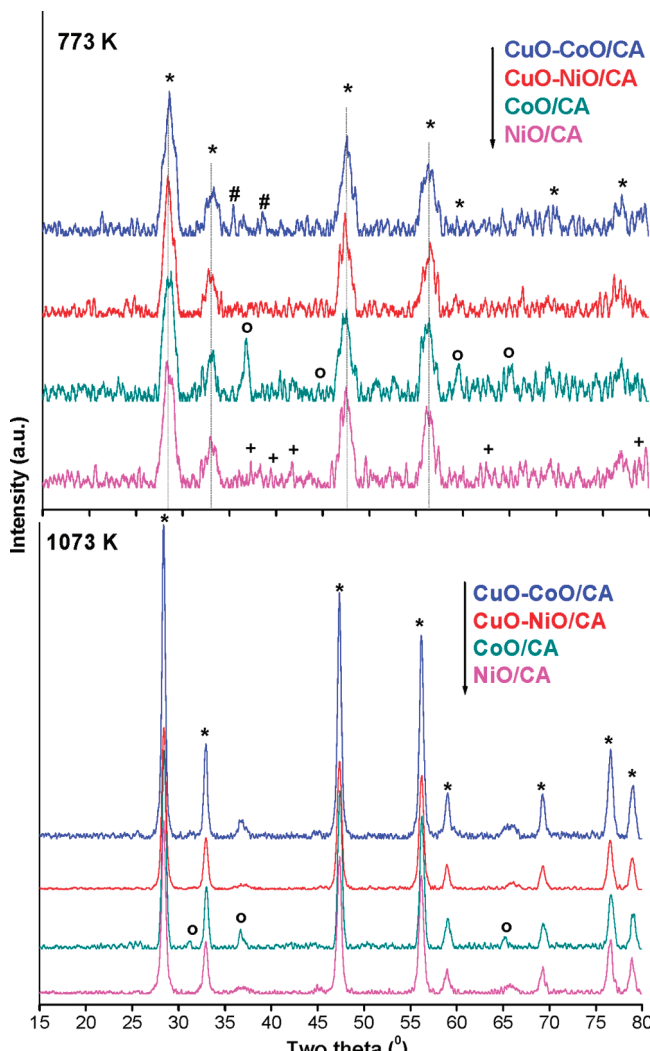


Figure 1. X-ray powder diffraction patterns of CuO–CoO/CeO₂–Al₂O₃, CuO–NiO/CeO₂–Al₂O₃, CoO/CeO₂–Al₂O₃, and NiO/CeO₂–Al₂O₃ samples calcined at 773 and 1073 K: (*) lines due to cubic CeO₂; (#) lines due to Co₃O₄; (o) lines due to CoO; (+) lines due to NiO.

of Al_2O_3 peaks in the XRD profiles suggest an amorphous nature of alumina.^{20,24} Additionally, no bulk crystalline phases corresponding to alumina and ceria compounds could be observed. According to the model proposed by Humbert et al.,³³ the geometrical arrangement between the three structures of CeO_2 , CeAlO_3 , and transition Al_2O_3 also favor the formation of cerium aluminate at the interface. However, in the present study, there is no evidence for the formation of the CeAlO_3 phase. In the case of monometallic CoO/CA sample, the observed peaks at $2\theta = 36.8^\circ, 44.8^\circ, 59.3^\circ$, and 65.2° (PDF-ICDD 43-1003) were assigned to the formation of a cubic Co_3O_4 spinel. Whereas, NiO/CA shows the characteristic peaks corresponding to NiO (PDF-ICDD 78-0429) appeared at $2\theta = 36.4^\circ, 39.02^\circ, 42.6^\circ, 62.2^\circ$, and 78.6° .^{34,35} The XRD pattern of the $\text{CuO}-\text{CoO}/\text{CA}$ sample exhibited two additional small peaks at $2\theta = 34.7^\circ$ and 37.9° that were interpreted as due to tenorite copper oxide (PDF-ICDD 45-0937).^{20,25} Interestingly, in the case of the $\text{CuO}-\text{NiO}/\text{CA}$ sample, no diffraction lines pertaining to the CuO phase were observed, which indicate that the addition of copper to nickel enhances the dispersion of copper. Further, it can be speculated that the dispersion of CuO is slightly higher in the $\text{CuO}-\text{NiO}/\text{CA}$ as compared to the $\text{CuO}-\text{CoO}/\text{CA}$ sample. In general, the poor intensity of the lines reveals that the prepared materials are mostly in an amorphous state.

The XRD patterns of various samples calcined at 1073 K (Figure 1) show major diffraction lines due to crystalline cubic phase of ceria (PDF-ICDD 34-0394). With an increase of the calcination temperature from 773 to 1073 K, an increase in the intensity of peaks pertaining to ceria has been observed. The increase in the intensity of the lines could be attributed to better crystallization of the samples under the effect of high temperature calcination. However, in cobalt containing samples three additional small peaks were observed, which suggest that some of the Co_3O_4 is in the crystalline form.^{5,36} Further, the absence of obvious diffraction lines due to CuO in the bimetallic samples suggests the existence of the smaller and extremely well-dispersed copper particles in the catalysts, which is in agreement with the previous studies.^{37,38} This could be also due to oxide solid solution formation or the copper phase being finely dispersed over the ceria–alumina.^{11,15,36} It is difficult to distinguish $\text{Cu}_x\text{Co}_{3-x}\text{O}_4$ phases from XRD measurements because its diffraction patterns are similar to the Co_3O_4 spinel.³⁹ In the next subsequent TPR studies, we have demonstrated the existence of a highly dispersed copper oxide clusters over the ceria–alumina support. The coexistence of clusters and CuO particles was also revealed by distinct TPR peaks. The XRD analyses of 1073 K calcined samples indicate the absence of copper oxide peaks that may be due to coexistence of CuO with ceria and/or other mixed metal oxides.

The reduction properties of the synthesized catalysts were investigated using TPR technique. The H_2 consumption profiles as a function of temperature are shown in Figure 2. As can be observed from the figure, the reduction behaviors of ceria and other oxides have been dramatically changed by the addition of copper. In general, the reduction peak pertaining to surface oxygen of CeO_2 appears at ~ 673 K.^{11,16,20} However, for copper promoted samples this peak shifted to lower temperatures and was observed at ~ 520 K. The CoO/CA sample exhibited two-stage broad reduction peaks, a low temperature peak at 510 K due to the reduction of dispersed Co^{3+} and a more intense broad prominent signal at 650 K related to bulk reduction of Co_3O_4 species.^{5,36} Recently, Todorova et al.³⁹ also reported a broad TPR peak for Co_3O_4 sample. Our results are in good agreement with their work.³⁹ It is a well-known fact that TPR peak shapes

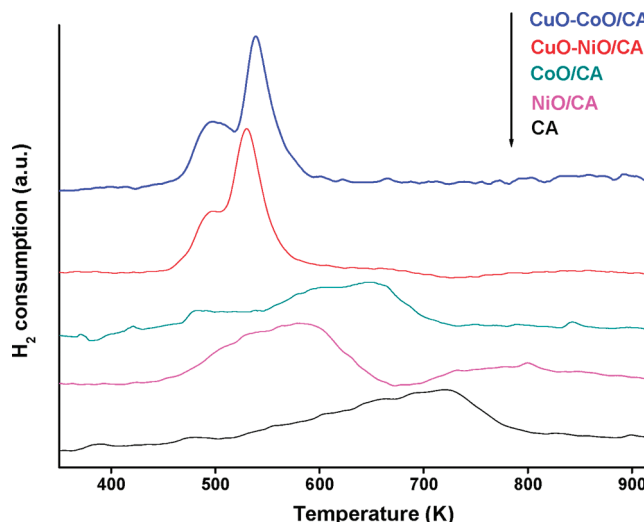


Figure 2. H_2 -TPR profiles of $\text{CeO}_2-\text{Al}_2\text{O}_3$, $\text{CuO}-\text{CoO}/\text{CeO}_2-\text{Al}_2\text{O}_3$, $\text{CuO}-\text{NiO}/\text{CeO}_2-\text{Al}_2\text{O}_3$, $\text{CoO}/\text{CeO}_2-\text{Al}_2\text{O}_3$, and $\text{NiO}/\text{CeO}_2-\text{Al}_2\text{O}_3$ samples calcined at 773 K.

and positions are highly sensitive to the experimental conditions employed in addition to the nature of the catalyst systems. The TPR profile of the NiO/CA sample shows a broad H_2 consumption peak ranging from 550 to 780 K, which consists of reduction profiles of both Ni^{2+} and surface cerium oxide.³⁵ The H_2 consumption profiles of Cu promoted bimetallic samples are completely distinct from the other monometallic samples as presented in Figure 2. The reducibility of Co_3O_4 and NiO has been shifted to lower temperatures, and the reduction profiles of cobalt and nickel coexist with the high temperature copper oxide peak. The TPR profiles of bimetallic catalysts are characterized by a prominent and rather sharp peak located at $T_{\max} = 530$ K and a shoulder peak at $T_{\max} = 495$ K. The first reduction peak that appeared at 495 K is due to the dispersed copper oxide, and the second sharp peak could be attributed to the reduction of crystalline CuO to Cu^0 .⁴⁰ Boyce et al.⁴¹ and Barrault et al.⁴² investigated the TPR profiles of CuO and NiO particles on different supports, such as CeO_2 , Al_2O_3 , and SiO_2 and reported that bulk CuO reduces at 473–573 K, while NiO reduces at 573–673 K. Similar results were noted for the $\text{CuO}-\text{NiO}/\text{CA}$ sample in the present study. On the other hand, the $\text{CuO}-\text{CoO}/\text{CA}$ sample exhibited a reduction signal centered at $T_{\max} = 540$ K, which is slightly higher in temperature than the $\text{CuO}-\text{NiO}/\text{CA}$ sample. It indicates the distribution of bigger copper particles which are slightly more in the $\text{CuO}-\text{CoO}/\text{CA}$ sample corroborating with the results observed from XRD study. On the whole, the TPR results are in good agreement with the XRD observations. Hence, Cu promoted bimetallic systems over ceria–alumina significantly promotes the reducibility and dispersion of metal oxides by strong interaction at the interface between copper and the surface oxygen vacancies of ceria. However, the presence of more than one reduction peak in the copper doped samples is an indication of the existence of more than one copper oxide species in the bimetallic systems. The synergistic interaction between the CuO and CeO_2 is more evident from a decrease in the reduction temperature of both CuO moieties and CA support. It can be concluded from H_2 -TPR experiments that Cu-doping decreases the onset reduction temperature of monometallic samples and enhances oxygen mobility within the lattice.

Raman spectroscopy is a powerful technique to gain understanding about the mobility of oxygen atoms in the ceria lattice and gather structural details.^{10,21,22} Accordingly, the Raman

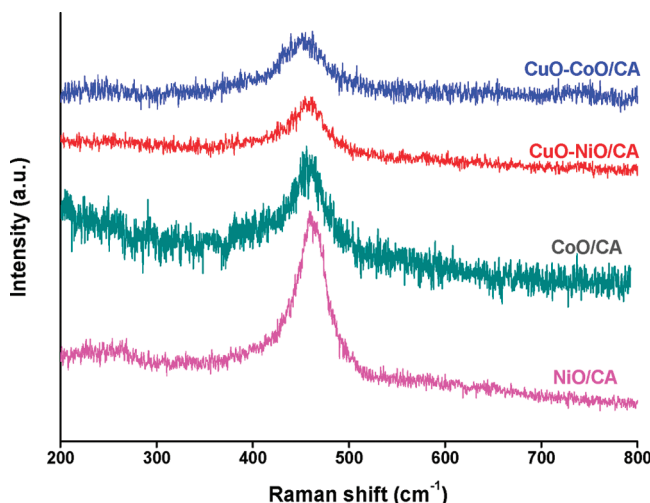


Figure 3. Raman spectra of CuO–CoO/CeO₂–Al₂O₃, CuO–NiO/CeO₂–Al₂O₃, CoO/CeO₂–Al₂O₃, and NiO/CeO₂–Al₂O₃ calcined at 773 K.

Table 2. Metal Loadings (wt %) from EDX and XPS Core Level Electron Binding Energies (eV) of Various Samples Calcined at 773 K

sample	metal loading (wt %)			binding energy (eV)				
	Cu	Co	Ni	Ce 3d _{5/2}	O 1s	Al 2p	Cu 2p _{3/2}	Co 2p _{3/2}
CoO/CA		9.60		882.3	532.4	74.2		782.1
NiO/CA			10.06	882.4	532.5	74.2		
CuO–NiO/CA	4.81		4.95	882.7	532.1	74.5	933.9	
CuO–CoO/CA	4.77	4.86		882.6	532.2	74.4	934.1	781.3

spectra of various samples prepared in this investigation have been recorded. As presented in Figure 3, the Raman spectra of various samples show a prominent broad peak at around 461 cm⁻¹. The Raman band at 461 cm⁻¹ corresponds to the triply degenerate F_{2g} mode and can be viewed as a symmetric breathing mode of oxygen atoms around cerium ions.^{19–23} In general, the broad band reflects the phonon density states, which is a characteristic of Raman scattering for amorphous materials. It is a known fact in the literature that the intensity of the Raman band depends on several factors including the grain size and morphology.²¹ A weak band is present at ~600 cm⁻¹ corresponding to a doubly degenerate LO mode of CeO₂, which is normally expected for free ceria only samples which are absent in the present study. Inline with XRD measurements, no Raman bands pertaining to the alumina or compounds of ceria and alumina were observed. Therefore, the Raman measurements suggest existence of a surface overlayer of ceria on the alumina support as envisaged earlier.²³

To obtain information about metal ions present and to assess the surface composition of the active components over the CA support, EDX investigation was performed on various samples calcined at 773 K. The quantities of active metal ions impregnated over the support are shown in Table 2. As expected, EDX results revealed the presence of Ce, Al, O, Co, Ni, and Cu elements in the respective mono- and bimetallic samples in appropriate proportions. The quantitative amounts of the metal loadings (in weight percent) obtained from EDX results are corroborating well with the actual metal loadings within the permissible limits. Obviously, these results suggest that all the active metal components impregnated over the CA are present on the catalyst surface.

To obtain the structural information at an atomic scale, the TEM studies were performed on some selected representative samples, which, on the other hand, can compliment the results obtained from other measurements. Figure 4A–C represents the

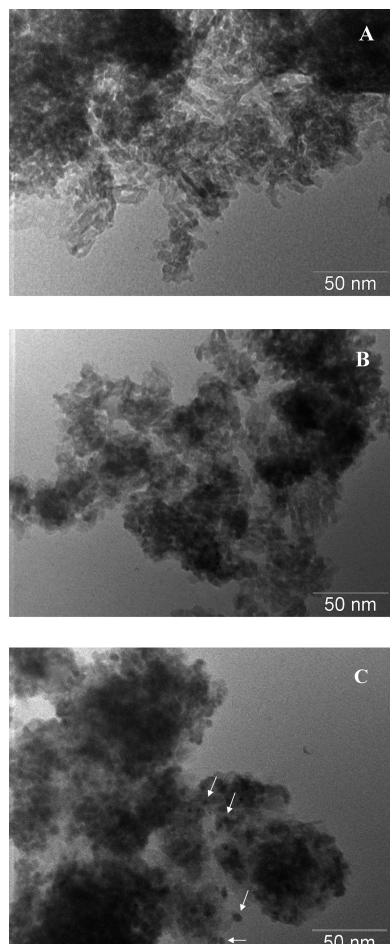


Figure 4. TEM images of CuO–NiO/CeO₂–Al₂O₃ (A), CuO–CoO/CeO₂–Al₂O₃ (B), and CoO/CeO₂–Al₂O₃ (C) calcined at 773 K.

textural features of CuO–NiO/CA, CuO–CoO/CA, and CoO/CA samples calcined at 773 K, respectively. Figure 4C displays the representative TEM image of the CoO/CA sample. As can be observed from the figure, homogeneously distributed within the narrow size range small cobalt particles were present on the catalyst surface (indicated by arrows). Whereas, bimetallic Cu-containing samples exhibited rode like morphology (Figure 4A and B) with equal particle size distribution. However, the particle sizes of CoO/CA mixed oxide ranged between 3 to 10 nm, and the bimetallic samples showed a distribution range from 5 to 13 nm. In particular, copper promoted samples revealed an increase in the particle size compared to that of monometallic samples. These observations are inline with mean crystallite sizes calculated from X-ray line broadening technique (Table 1). It was identified that synthesis of uniform and equally distributed particles can significantly improve the catalytic activity in mixed oxide systems. In the present study, the small particle size and narrow size distribution may be associated to fast nucleation and slow growth process, which regulates the particle size of the catalysts.⁴³

XPS data provides information about the surface composition obtained from core photoemission intensity data and the chemical state of elements in the near-surface region. Binding energies (BE) of the selected photoemission lines of various catalysts are summarized in Table 2. The core level photoelectron peaks of Cu 2p and Co 2p are depicted in Figure 5A and B, respectively. As presented in Figure 5A, the Cu 2p_{3/2} signal is composed of two combination peaks at 932.8 and 934.6 eV. In addition to these signals, a shakeup satellite peak is observed

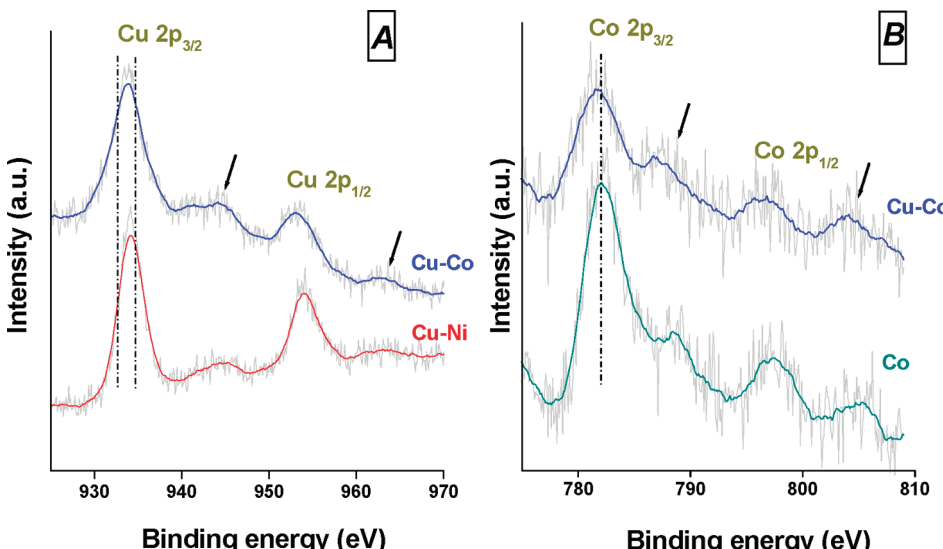


Figure 5. (A) Cu 2p core level XP spectra of CuO–CoO/CeO₂–Al₂O₃ (Cu–Co) and CuO–NiO/CeO₂–Al₂O₃ (Cu–Ni) samples. (B) Co 2p core level XP spectra of CuO–CoO/CeO₂–Al₂O₃ (Cu–Co) and CoO/CeO₂–Al₂O₃ (Co) samples.

in the region of 941–946 eV. According to previous XPS studies, the features, such as spin–orbit splitting and shakeup satellite, should be used for identifying the transition metals oxidation state.^{44–47} The intense peak at 934.3 eV could be attributed to the CuO moiety and the lower binding energy peak at 933.1 eV has been assigned to the presence of Cu¹⁺, which is close to the one reported earlier for pure Cu₂O (932.8 eV).⁴⁵ According to Batista et al.,⁴⁶ only Cu²⁺ species shows a shakeup satellite peak located about 10 eV higher than the Cu 2p_{3/2} transition; this characteristic peak is used to differentiate between Cu²⁺ and reduced copper. The intensity ratios of the shakeup satellite to the corresponding principal peak ($I_{\text{sat}}/I_{\text{pp}}$) for CuO–NiO/CA and CuO–CoO/CA catalysts has been calculated and was found to be 0.12 and 0.14, respectively. This is between the value of 0.55, the characteristic value for pure Cu²⁺, and 0, which corresponds to Cu¹⁺ species, and indicates that both the bimetallic catalysts contain CuO and Cu₂O as Cu–O–Ce species on the catalytic surface.⁴⁷ However, the bimetallic copper–nickel catalyst exhibited slightly more intense principal peaks (Cu 2p_{3/2} and Cu 2p_{1/2}) and low intense shakeup satellite signals compared to the copper–cobalt sample. Therefore, the intensity of satellite peaks and the ratio between $I_{\text{sat}}/I_{\text{pp}}$ indicates the existence of higher amounts of Cu¹⁺ ions in CuO–NiO/CA sample. Liu et al.¹⁶ proposed an interfacial interaction for Cu–O–Ce catalyst; the copper ions at the interfacial region of the finely dispersed CuO clusters and CeO₂ can penetrate into the cerium oxide lattice by occupying the vacant sites of the cerium ions. Furthermore, the thermogravimetry, TPR, and XRD results also suggested the synergistic interface interactions between copper and ceria.

Figure 5B represents the XP spectrum of the Co 2p region of CoO/CA and CuO–CoO/CA samples. The presence of Co²⁺ is confirmed by the Co 2p_{3/2} peak at 781.3 eV, accompanied by a relatively intense 3d → 4s shakeup satellite peak at 787 eV in the CuO–CoO/CA sample.^{39,44–48} The spin–orbit splitting upon ionization between 2p_{3/2} and 2p_{1/2}, that is ca. 15.7 eV, was also observed. However, the CoO/CA sample shows an intense peak at 782.1 eV with a satellite peak at 788.4 eV. In general, these peaks were explained as being due to the presence of both Co₃O₄ and CoAl₂O₄.⁴⁹ Interestingly, the absence of CoAl₂O₄ compound in the bimetallic sample discloses that the addition of copper to cobalt prevents the enrichment Co in the alumina lattice; i.e. the addition of copper suppresses the

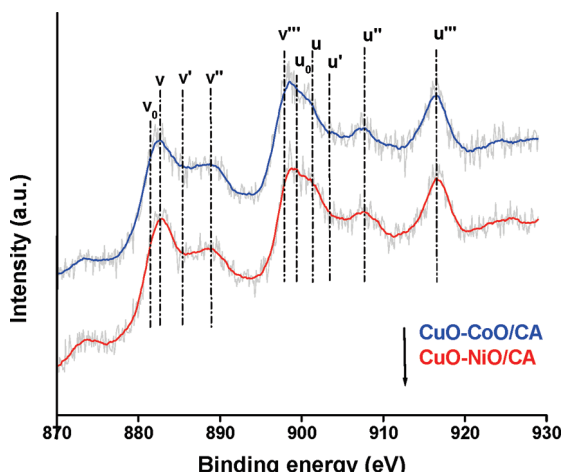


Figure 6. Ce 3d XP spectra of bimetallic CuO–CoO/CeO₂–Al₂O₃ and CuO–NiO/CeO₂–Al₂O₃ samples calcined at 773 K.

CoAl₂O₄ formation. In the bimetallic sample, the Co 2p_{3/2} peak is shifted to lower binding energy compared to the monometallic sample and the satellite peak is registered as a shoulder. The decrease in the shakeup peak typically is due to the existence of the Co₃O₄ spinel with the mixed valence of cobalt. In general, Co₃O₄ contains two distinct types of cobalt ions: Co²⁺ in tetrahedral sites and Co³⁺ in octahedral sites, in the ratio of 1:2.^{44,45} As the 2p_{3/2} binding energies of Co²⁺ are relatively close to that of Co³⁺, the two oxidation states of cobalt must be distinguished by the presence of a distinct shakeup satellite structure in Co²⁺. These results are in agreement with the TPR and XRD data. The shift to lower binding energy values are, probably, from the increase in the valence state of Co.

As shown in Figure 6, the Ce 3d profile is more complicated due to mixing of Ce 4f levels with O 2p states. The notation of the Ce 3d peaks in the present study has been envisaged as elucidated in the literature.⁵⁰ Two sets of spin–orbit multiplets, corresponding to the 3d_{3/2} and 3d_{5/2} contributions are labeled as *u* and *v*, respectively. As shown in the figure, the Ce 3d spectrum is integrated to subsequent peaks at about 881.3 (V₀), 882.6 (V), 888.9 (V'), 897.5 (V''), 899.2 (u₀), 901.0 (u), 907.5 (u''), and 916.5 eV (u'''). The principal peaks of 3d_{5/2} and 3d_{3/2} are located at 882.6 and 901 eV, respectively. The peaks *v''*

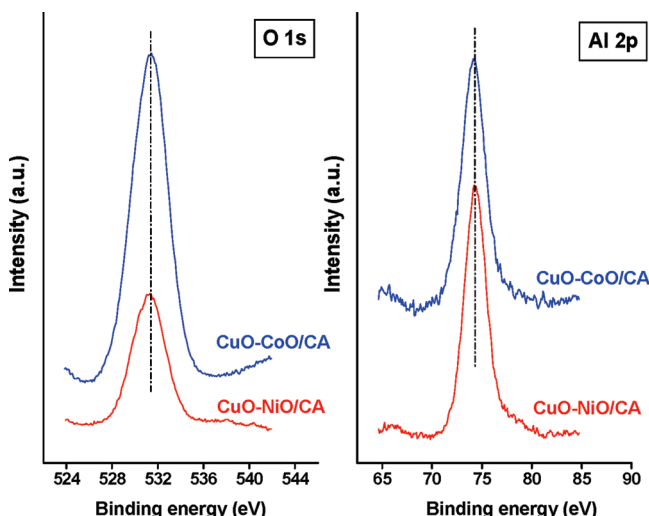


Figure 7. O 1s and Al 2p XP spectra of bimetallic CuO–CoO/CeO₂–Al₂O₃ and CuO–NiO/CeO₂–Al₂O₃ samples calcined at 773 K.

and ν'' are the satellites arising from ionization of Ce 3d_{5/2}, while the signals u'' and u''' are accounting for ionization of Ce 3d_{3/2}. Recent studies on ceria-based materials reveal that the peaks at 903.2–903.5 and 884.7–885.0 eV represent the 3d¹⁰ 4f¹ initial electronic states corresponding to Ce³⁺, whereas the peaks at 915.9–916.1 and 897.5–897.8 eV reveal the 3d¹⁰ 4f¹ state of Ce⁴⁺ ions.^{21–23} However, in the present investigation, peaks corresponding to Ce⁴⁺ are observed predominantly, indicating the main valence of cerium in the synthesized samples is 4+. The electron binding energies of Ce 3d_{5/2} of various samples are shown in Table 2. It can be observed from Table 2 that both mono- and bimetallic samples exhibit similar Ce 3d_{5/2} binding energy values with a slight variation. The small difference in the binding energies could be due to different metal ions' environments near the cerium sites.

The O 1s and Al 2p spectrum of copper promoted bimetallic samples are shown in Figure 7. As can be noted from the O 1s profiles, the existence of broad and complicated peaks are due to overlapping contributions of oxygen from ceria–alumina mixed oxide and the corresponding metal oxide loaded samples, respectively. It is a known fact that the broadening of XPS peak depends on various factors including (i) the presence of more than one type of species with different chemical characteristics which cannot be discerned by XPS and (ii) electron transfer between the active metal oxide and the support. The observed intense peak at ~532.1 eV is primarily belongs to the oxygen atoms that are bound to the cerium ions.^{21–24} However, the cobalt containing sample exhibited high intense peak, generally, it is due to the availability of high concentration of cobalt oxide and/or the overlapping contribution from the Co₃O₄ spinel.^{45,46,49} As presented in Figure 7, the binding energy of the Al 2p photoelectron peak ranged between 70.1 and 78.7 eV for both CuO–NiO/CA and CuO–CoO/CA samples, which agrees well with the literature reports.²¹ It could be observed that the XP spectra of alumina are relatively broad, which indicates that alumina is not easily accessible at the surface due to the presence of the ceria overlayer. However, a reasonably good intensity of the Al 2p peak is mainly due to better crystallization and redistribution of various components in the samples under calcination treatment. Thus, the XPS results provide adequate information on the surface composition of different metal components that constitute the catalysts.

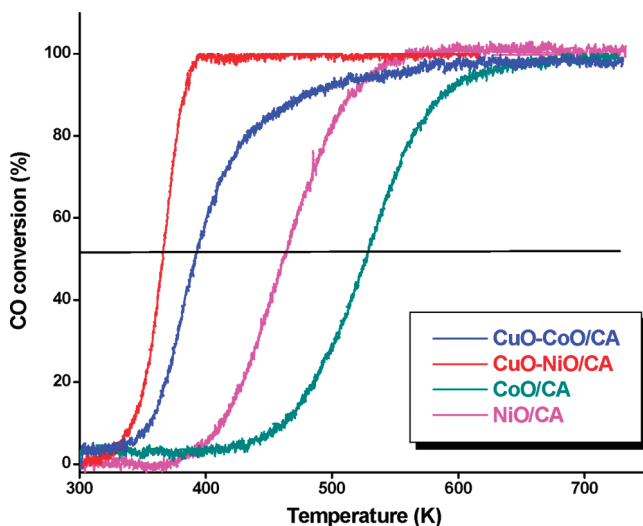


Figure 8. CO conversion as a function of temperature over CuO–CoO/CeO₂–Al₂O₃, CuO–NiO/CeO₂–Al₂O₃, CoO/CeO₂–Al₂O₃, and NiO/CeO₂–Al₂O₃ samples calcined at 773 K.

3.2. Activity Studies. The catalytic behavior for CO oxidation of the synthesized mono- and bimetallic catalysts calcined at 773 K is shown in Figure 8. In this reaction carbon dioxide is the sole product and the conversion of CO is defined as the percentage of CO to be converted into CO₂. Before the CO activity measurements, pretreatment of the catalyst was carried out in an oxygen atmosphere because O₂ pretreatment causes an enrichment of the oxygen storage on the Cu active species and promotes the conversion of adsorbed oxygen into surface lattice oxygen. In addition, Zou et al.⁵¹ showed that the Cu–Zr–Ce–O catalyst pretreated with oxygen exhibits the best catalytic performance and had the widest operating temperature window. To compare the activity of various samples, the obtained results are listed in Table 1 ($T_{1/2}$). $T_{1/2}$ represents the temperature at 50% conversion of CO (light-off temperature). As could be seen from Figure 8, the conversion of CO linearly increases with rise in the reaction temperature for all the catalyst systems. The light-off temperatures for CuO–NiO/CA and CuO–CoO/CA catalysts are 364 and 392 K, respectively. There is a lowering of $T_{1/2}$ around 100 K in the case of the CuO–NiO/CA sample compared to monometallic NiO/CA sample. Similar enhanced activity was observed for Cu promoted CoO/CA sample, where the $T_{1/2}$ is decreased to about 130 K. Moreover, bimetallic catalysts exhibited ~100% conversion at below 600 K, which indicates that the copper promoted samples are promising materials for CO oxidation.

The Mars–van Krevelen mechanism (MVK) has been suggested for CO oxidation over CeO₂ containing copper catalysts on the basis of detailed kinetic measurements.^{52,53} Furthermore, several works already proposed some theories about the synergism between copper and cerium in the Cu–CeO₂ catalysts. In such models, CO adsorption is supposed to take place on the copper sites while ceria provides the lattice oxygen. In this way, the oxidation reaction proceeds at the metal–support interface. In conclusion, some authors reported that synergistic effects would involve stabilization by ceria support of nonstoichiometric metastable copper oxide species formed during the reaction, which species would be highly active for the CO oxidation reaction.^{11,51–53} However, in the present investigation addition of copper significantly reduced the temperature of complete oxidation, and also, the CuO promoted bimetallic catalysts showed 100% CO conversion. These observations suggest that the strong interaction between copper

and ceria is responsible for the enhancement of low temperature activity of CO oxidation. Among the examined bimetallic nanocomposite oxide catalysts, CuO–NiO/CA exhibited markedly enhanced catalytic activity which could be attributed to synergetic interactions between copper oxide and ceria as well as existence of Cu¹⁺ ions over the surface. Combined results of XRD, TEM, TPR, Raman spectra, and XPS provided information regarding the influence of copper on monometallic Ni and Co samples over CA support and also revealed that the finely dispersed and highly reducible metal species mainly contributes to the catalytic activity.

4. Conclusions

Copper promoted CuO–CoO/CeO₂–Al₂O₃ and CuO–NiO/CeO₂–Al₂O₃ catalysts were synthesized by deposition precipitation followed by the wet impregnation method and calcined at 773 and 1073 K. Thermogravimetric analysis of the synthesized samples indicated that the prepared catalysts are thermally stable up to 1100 K, while the cobalt containing sample exhibited reduction of Co₃O₄ spinel to CoO at about 1130 K. The BET surface area results revealed that all samples exhibited moderately high specific surface areas of about 140 m² g⁻¹. The X-ray diffraction profiles of 773 K calcined samples revealed the presence of specific metal oxide phases in the corresponding catalysts. Interestingly, at higher calcination temperatures, there are no peaks pertaining to the impregnated metal oxides, which revealed that the impregnated metal oxides are well distributed over the support surface and are stable even at higher temperatures. The TPR studies of Cu-promoted bimetallic systems showed well dispersed metal oxides by strong interaction at the interface between copper and the surface oxygen vacancies of ceria. Raman measurements revealed the existence of a surface overlayer of ceria on the alumina support. The TEM studies confirmed the presence of nanosized composite oxides within the narrow size distribution of metal oxide particles. The Cu 2p photoelectron peaks disclosed the presence of Cu¹⁺ species along with Cu²⁺ ions. Furthermore, the XP spectrum of Co 2p revealed that doping of copper to cobalt containing sample suppresses the formation of CoAl₂O₄ phase. Among various samples investigated, the copper promoted CuO–NiO/CeO₂–Al₂O₃ sample exhibited high activity for CO oxidation with a $T_{1/2}$ of 364 K. The better activity of the sample is attributed to finely dispersed and highly reducible metal species over the catalyst surface.

Acknowledgment

K.N.R. and P.B. thank the University Grants Commission (UGC), New Delhi, and Council of Scientific & Industrial Research (CSIR), New Delhi, for Senior Research Fellowships, respectively.

Supporting Information Available: More details of thermogravimetric profiles of different catalyst systems before calcination. This material is available free of charge via the Internet at <http://pubs.acs.org>.

Literature Cited

- (1) Seshan, K.; Lercher, J. A. Carbon Dioxide Chemistry: Environmental Issues. *R. Soc. Chem.* **1994**, 16.
- (2) Fu, Q.; Saltsburg, H.; Flytzani-Stephanopoulos, M. Active nonmetallic Au and Pt species on ceria-based water-gas shift catalysts. *Science* **2003**, 301, 935–938.
- (3) Gardner, S. D.; Hoflund, G. B.; Schtyer, D. R.; Schryer, J.; Upchurch, B. T.; Kielin, E. J. Catalytic behavior of noble metal/reducible oxide materials for low-temperature carbon monoxide oxidation. I. Comparison of catalyst performance. *Langmuir* **1991**, 7, 2135–2139.
- (4) Woitsch, A.; Descorme, C.; Duprez, C. Preferential oxidation of carbon monoxide in the presence of hydrogen (PROX) over ceria-zirconia and alumina-supported Pt catalysts. *J. Catal.* **2004**, 225, 259–266.
- (5) Yao, Y.-F. Y. The oxidation of hydrocarbons and CO over metal oxides: III. Co₃O₄. *J. Catal.* **1974**, 33, 108–122.
- (6) Watanabe, M.; Uchida, H.; Igarashi, H.; Suzuki, M. Pt catalyst supported on zeolite for selective oxidation of CO in reformed gases. *Chem. Lett.* **1995**, 21–22.
- (7) Igarashi, H.; Ushida, H.; Suzuki, M.; Sasaki, Y.; Watanabe, M. Removal of carbon monoxide from hydrogen-rich fuels by selective oxidation over platinum catalyst supported on zeolite. *Appl. Catal., A* **1997**, 159, 159–169.
- (8) Schubert, M. M.; Kahlich, M. J.; Gasteiger, H. A.; Behm, R. Correlation between CO surface coverage and selectivity/kinetics for the preferential CO oxidation over Pt/γ-Al₂O₃ and Au/α-Fe₂O₃: an in-situ DRIFTS study. *J. Power Sources* **1999**, 84, 175–182.
- (9) Lin, W.; Flytzani-Stephanopoulos, M. Total oxidation of carbon monoxide and methane over transition metal fluorite oxide composite catalysts: I. Catalyst composition and activity. *J. Catal.* **1995**, 153, 304–316.
- (10) Reddy, B. M.; Bharali, P.; Saikia, P.; Thrimurthulu, G.; Yamada, Y.; Kobayashi, T. Thermal stability and dispersion behavior of nanostructured Ce_xZr_{1-x}O₂ mixed oxides over anatase-TiO₂: a combined study of CO oxidation and characterization by XRD, XPS, TPR, HREM, and UV-vis DRS. *Ind. Eng. Chem. Res.* **2009**, 48, 453–462.
- (11) Wang, X.; Rodriguez, J. A.; Hanson, J. C.; Gamarra, D.; Martinez-Arias, A.; Fernandez-Garcia, M. Unusual physical and chemical properties of Cu in Ce_{1-x}Cu_xO₂ oxide. *J. Phys. Chem. B* **2005**, 109, 19595–19603.
- (12) Taylor, C. E.; Howard, B. H.; Myers, C. R. Methanol conversion for the production of hydrogen. *Ind. Eng. Chem. Res.* **2007**, 46, 8906–8909.
- (13) Knauth, P.; Schwitzgebel, G.; Tschöpe, A.; Villain, S. EMF measurements on nanocrystalline copper-doped ceria. *J. Solid State Chem.* **1998**, 140, 295–299.
- (14) Shen, G.-C.; Fujita, S.-I.; Matsumoto, S.; Takezawa, N. Steam reforming of methanol on binary Cu/ZnO catalysts: Effects of preparation condition upon precursors, surface structure and catalytic activity. *J. Mol. Catal. A* **1997**, 124, 123–136.
- (15) Avgoustopoulos, G.; Ioannides, T.; Papadopoulou, C.; Batista, J.; Hocevar, S.; Matralis, H. K. A comparative study of Pt/γ-Al₂O₃, Au/α-Fe₂O₃ and CuO-CeO₂ catalysts for the selective oxidation of carbon monoxide in excess hydrogen. *Catal. Today* **2002**, 75, 157–167.
- (16) Liu, W.; Flytzani-Stephanopoulos, M. Total oxidation of carbon monoxide and methane over transition metal fluorite oxide composite catalysts: ii. Catalyst characterization and reaction-kinetics. *J. Catal.* **1995**, 153, 317–332.
- (17) Kim, D. H.; Cha, J. E. A CuO-CeO₂ mixed oxide catalyst for CO clean-up by selective oxidation in hydrogen-rich mixtures. 9th APCCHE Congress, Christchurch, New Zealand, Sept 29 to October 3, 2002; p 619.
- (18) Han, Y.-F.; Kahlich, M. J.; Kinne, M.; Behm, R. J. Kinetic study of selective CO oxidation in H₂-rich gas on a Ru/γ-Al₂O₃ catalyst. *Phys. Chem. Chem. Phys.* **2002**, 4, 389–397.
- (19) Trovarelli, A.; Zamar, F.; Llorca, J.; De Leitenburg, C.; Dolcetti, G.; Kiss, J. T. Nanophase fluorite-structured CeO₂-ZrO₂ catalysts prepared by high-energy mechanical milling. *J. Catal.* **1997**, 169, 490–502.
- (20) Martinez-Arias, A.; Cataluña, R.; Conesa, J. C.; Soria, J. Effect of copper-ceria interactions on copper reduction in a Cu/CeO₂/Al₂O₃ catalyst subjected to thermal treatments in CO. *J. Phys. Chem. B* **1998**, 102, 809–817.
- (21) Reddy, B. M.; Rao, K. N.; Reddy, G. K.; Khan, A.; Park, S.-E. Structural characterization and oxide hydrogenation activity of CeO₂/Al₂O₃ and V₂O₅/CeO₂/Al₂O₃ catalysts. *J. Phys. Chem. C* **2007**, 111, 18751–18758.
- (22) Reddy, B. M.; Bharali, P.; Saikia, P.; Park, S.-E.; van den Berg, M. W. E.; Muhler, M.; Gruenert, W. Structural characterization and catalytic activity of nanosized Ce_xM_{1-x}O₂ (M = Zr and Hf) mixed oxides. *J. Phys. Chem. C* **2008**, 112, 11729–11737.
- (23) Reddy, B. M.; Saikia, P.; Bharali, P. Highly dispersed Ce_xZr_{1-x}O₂ nano-oxides over alumina, silica and titania supports for catalytic applications. *Catal. Surv. Asia* **2008**, 12, 214–228.
- (24) Reddy, B. M.; Reddy, G. K.; Rao, K. N.; Katta, L. Influence of alumina and titania on the structure and catalytic properties of sulfated zirconia: Beckmann rearrangement. *J. Mol. Catal. A* **2009**, 306, 62–68.
- (25) Kang, M.; Song, M. W.; Lee, C. H. Catalytic carbon monoxide oxidation over CoO_x/CeO₂ composite catalysts. *Appl. Catal., A* **2003**, 251, 143–156.

- (26) Mariño, F.; Descorme, C.; Duprez, D. Supported base metal catalysts for the preferential oxidation of carbon monoxide in the presence of excess hydrogen (PROX). *Appl. Catal., B* **2005**, *58*, 175–183.
- (27) Briggs, D.; Seah, M. P. Practical Surface Analysis. In *Auger and X-Ray Photoelectron Spectroscopy*, 2nd ed.; Wiley: New York, 1990; Vol. 1.
- (28) Wagner, C. D.; Riggs, W. M.; Davis, L. E.; Moulder, J. F. In *Handbook of X-Ray Photoelectron Spectroscopy*; Muilenberg, G. E., Ed.; PerkinElmer Corporation: Waltham, MA, 1978.
- (29) Sundararajan, R.; Srinivasan, V. Catalytic decomposition of nitrous oxide on Cu_xCo_{3-x}O₄ spinels. *Appl. Catal.* **1991**, *73*, 165–171.
- (30) Porta, P.; Dragone, R.; Fierro, G.; Inversi, M.; Jacono, M. L.; Moretti, G. Preparation and characterisation of cobalt-copper hydroxysalts and their oxide products of decomposition. *J. Chem. Soc., Faraday Trans. 1* **1992**, *88*, 311–319.
- (31) Shaheen, W. M.; Ali, A. A. Characterization of solid-solid interactions and physico-chemical properties of copper-cobalt mixed oxides and Cu_xCo_{3-x}O₄ spinels. *Mater. Res. Bull.* **2001**, *36*, 1703–1716.
- (32) Bond, G. C.; Tahir, S. F. Vanadium oxide monolayer catalysts preparation, characterization and catalytic activity. *Appl. Catal.* **1991**, *71*, 1–31.
- (33) Humbert, S.; Colin, A.; Monceaux, L.; Ovdet, F.; Courtine, P. Simultaneous atmosphere and temperature cycling of three-way automotive exhaust catalysts. *Stud. Surf. Sci. Catal.* **1995**, *96*, 829–839.
- (34) Villa, R.; Cristiani, C.; Groppi, G.; Lietti, L.; Forzatti, P.; Cornaro, U.; Rossini, S. Ni based mixed oxide materials for CH₄ oxidation under redox cycle conditions. *J. Mol. Catal. A* **2003**, *204*, 637–646.
- (35) Alberton, A. L.; Souza, M. M. V. M.; Schmal, M. Carbon formation and its influence on ethanol steam reforming over Ni/Al₂O₃ catalysts. *Catal. Today* **2007**, *123*, 257–264.
- (36) Harrison, P. G.; Ball, I. K.; Daniell, W.; Lukinskas, P.; Céspedes, M.; Miró, E. E.; Ulla, M. A. Cobalt catalysts for the oxidation of diesel soot particulate. *Chem. Eng. J.* **2003**, *95*, 47–55.
- (37) Sinha, A. S. K.; Shanker, V. Low-temperature catalysts for total oxidation of n-hexane. *Ind. Eng. Chem. Res.* **1993**, *32*, 1061–1065.
- (38) Zhu, T.; Dreher, A.; Flytzani-Stephanopoulos, M. Direct reduction of SO₂ to elemental sulfur by methane over ceria-based catalysts. *Appl. Catal., B* **1999**, *21*, 103–120.
- (39) Todorova, S.; Kadinov, G.; Tenchev, K.; Kalvachev, Y.; Kytin, Y.-K. Particle size and support effects on the complete benzene oxidation by Co and Co-Pt catalysts. *J. Mater. Sci.* **2007**, *42*, 3315–3320.
- (40) Decarne, C.; Abi-Aad, E.; Kostyuk, B. G.; Lunin, V. V.; Aboukais, A. Characterization of cerium and copper species in Cu-Ce-Al oxide systems by temperature programmed reduction and electron paramagnetic resonance. *J. Mater. Sci.* **2004**, *39*, 2349–2356.
- (41) Boyce, A. L.; Graville, S. R.; Sermon, P. A.; Vong, M. S. W. Reduction of CuO-containing catalysts, CuO: I: TPR and TGA. *React. Kinet. Catal. Lett.* **1991**, *44*, 1–18.
- (42) Barrault, J.; Alouche, A.; Paul-Boncour, V.; Hilaire, L.; Percheron-Guegan, A. Influence of the support on the catalytic properties of nickel/ceria in carbon monoxide and benzene hydrogenation. *Appl. Catal.* **1989**, *46*, 269–279.
- (43) Ramaswamy, V.; Haynes, T. E.; White, C. W.; Moberly Chan, W. J.; Roorda, S.; Aziz, M. J. Synthesis of nearly monodisperse embedded nanoparticles by separating nucleation and growth in ion implantation. *Nano Lett.* **2005**, *5*, 373–377.
- (44) Cheng, J.; Yu, J.; Wang, X.; Li, L.; Li, J.; Hao, Z. Novel CH₄ combustion catalysts derived from Cu-Co/X-Al (X = Fe, Mn, La, Ce) hydrotalcite-like compounds. *Energy Fuels* **2008**, *22*, 2131–2137.
- (45) Fierro, J. L. G.; Jacono, M. L.; Inversi, M.; Dragone, R.; Porta, P. TRP and XPS study of cobalt-copper mixed oxide catalysts: evidence of strong Co-Cu interaction. *Top. Catal.* **2000**, *10*, 39–48.
- (46) Batista, J.; Pintar, A.; Mandrino, D.; Jenko, M.; Martin, V. XPS and TPR examinations of γ -alumina-supported Pd-Cu catalysts. *Appl. Catal., A* **2001**, *206*, 113–124.
- (47) Martinez-Arias, A.; Hungria, A. B.; Fernandez-Garcia, M.; Conesa, J. C.; Munuera, G. Preferential oxidation of CO in a H₂-rich stream over CuO/CeO₂ and CuO/(Ce, M)O_x (M = Zr, Tb) catalysts. *J. Power Sources* **2005**, *151*, 32–42.
- (48) Dudfield, C. D.; Chen, R.; Adcock, P. L. A carbon monoxide PROX reactor for PEM fuel cell automotive application. *Int. J. Hydrogen Energy* **2001**, *26*, 763–775.
- (49) Khassin, A. A.; Yurieva, T. M.; Kaichev, V. V.; Bukhitiarov, V. I.; Budneva, A. A.; Paukshits, E. A.; Parmon, V. N. Metal-support interactions in cobalt-aluminum co-precipitated catalysts: XPS and CO adsorption studies. *J. Mol. Catal.* **2001**, *175*, 189–204.
- (50) Silvestre-Albero, J.; Rodriguez-Reinoso, F.; Sepulveda-Escribano, A. Improved metal-support interaction in Pt/CeO₂/SiO₂ catalysts after zinc addition. *J. Catal.* **2002**, *210*, 127–136.
- (51) Zou, H.; Chen, S.; Lin, L. Effect of pretreatment methods on the performance of Cu-Zr-Ce-O catalyst for CO selective oxidation. *J. Natural Gas Chem.* **2008**, *17*, 208–211.
- (52) Sedmak, G.; Hocevar, S.; Levec, J. Kinetics of selective CO oxidation in excess of H₂ over the nanostructured Cu_{0.1}Ce_{0.9}O_{2-y} catalyst. *J. Catal.* **2003**, *213*, 135–150.
- (53) Qi, X.; Flytzani-Stephanopoulos, M. Activity and stability of Cu-CeO₂ catalysts in high-temperature water-gas shift for fuel-cell applications. *Ind. Eng. Chem. Res.* **2004**, *43*, 3055–3062.

Received for review May 10, 2009
Revised manuscript received August 4, 2009
Accepted August 5, 2009

IE900755B